Table of Contents

Part I: Supplementary Methods

Patient Selection for comparison of HCT versus CAR

Consecutive subjects receiving engineered cell therapies at Stanford Healthcare were enrolled after informed consent within a protocol reviewed and approved by the Stanford Institutional Review Board, with baseline clinical data collection centrally managed. Blood samples were collected per protocol at baseline (Day 0; D0), on D+7 (± 2), D+14 (± 4), D+21 (± 4), and D+28 (± 4). Control samples were collected from healthy adult blood donors, or from subjects with early-stage lymphoma at the time of their initial workup as part of clinically necessary testing. In addition, positive control specimens included bone marrow aspirates from subjects being evaluated for cytopenias after CAR therapy, as well as negative control bone marrow aspirates from subjects not receiving CAR therapy.

Propensity Matched HCT vs CAR analysis:

Data reporting follows the STROBE checklist for cohort studies. CAR-treated (n = 236) and HCT treated patients (n = 235) were screened from 01/2018-07/2022 and followed for a minimum of 90 days with 97.3% of CAR patients treated with standard of care similar to our prior analysis[1]. Patients were eligible for matching if they 1) were treated for LBCL, 2) had no documented LBCL relapse, and 3) had no prior cellular therapy. Patients were matched based on age, sex, prior lines of therapy, and time from infusion using the MatchIt[2] R algorithm using 1:1 nearest neighbor matching with a caliper set to 0.25 and successful matching considered as a standardized mean difference < 0.1. Propensity matched data updates were frozen as of 11/2022 and additional follow up present in subsequent analysis was not considered in the matched study. Last contact was defined as last contact noted in the electronic medical record. Death was defined as death from any cause.

Infection data was collected according to standard guidelines[3] with all infections manually reviewed and graded. Time to infection was defined as the first documentation in the medical record corresponding to the maximum CTCAE infection grade. Grading was performed according to CTCAE V5 with COVID definitions following the “other infections” grading criteria as recommended. Competing risk regression was performed in R using the cmprks2 package. Competing risks for infection were death from any cause or systemic chemotherapy treatment for second primary malignancy. For matched analysis both infection risk and survival were calculated at D+30 to prevent confounding from cytokine release syndrome during acute CAR toxicities and patients who did not survive to D+30 (n = 1 CAR patient) were excluded from analysis.

For immune reconstitution analysis patient complete blood count (CBC) data was reviewed manually in the electronic medical record. Time points were chosen to coincide with standard clinic visits for both therapies though broader timepoint windows were allowed to reduce data missingness. To account for variability in collection timepoints, time was treated as a categorical variable during analysis. Immune recovery was measured using multivariate linear mixed effects modeling as previously described[1]. Multivariate parameters included age, sex, systemic lines of therapy, and cell therapy type. Only timepoints from D28-D800 were considered to reduce confounding from initial conditioning and lymphodepleting chemotherapy as well as early immune reconstitution.

For each marker (WBC, ANC, ALC, HG, PLT) we fit a linear mixed-effects model with a patient-specific random intercept to account for within-patient correlation. The fixed-effects structure

included a main effect of Day (categorical; reference D28), main effects of treatment cohort (CCT Type: CAR vs HCT), age, sex, and number of prior systemic lines, and interactions between Day and each covariate:

$$Y_{ij} = \beta_0 + \alpha_{d[j]} + \gamma^{\top} X_i + \delta_{d[j]}{}^{\top} X_i + b_i + \varepsilon_{ij}$$

where X_i = (CCT Type$_i$, Age$_i$, Sex$_i$, Systemic Lines$_i$), $b_i \sim N\ (0, \sigma_b{}^2)$ and $\varepsilon_{ij} \sim N\ (0, \sigma^2)$

In R notation this is: Y Day * (CCT Type + Age + Sex + Systemic Lines) + (1|PID).

Models were fit by restricted maximum likelihood (REML) using lme4/lmerTest. Type-III tests for fixed effects were obtained from lmerTest; Kenward–Roger degrees of freedom were used when available, otherwise Satterthwaite. Adjusted means (estimated marginal means; emmeans) were computed by Day and CCT Type. To summarize recovery over the full window, we formed a single time-weighted CAR–HCT contrast by averaging the Day-specific adjusted differences using trapezoidal weights proportional to the gaps between scheduled days from D28 to D800 (larger gaps receive larger weight); CIs and p-values for contrasts used the same df method. Families of Day-wise tests were Holm-adjusted; the single time-weighted average was left unadjusted. Analyses used all available observations without imputation. The same results were obtained when Day was equally weighted. As sensitivity checks, we also performed a pre-specified Day-90 Wilcoxon comparison and an area-under-the-curve summary.

Assessment of clinical bone marrow and tMN data

Bone marrows were longitudinally collected from Stanford patients undergoing CAR T-cell treatment for non-Hodgkin lymphoma following IRB protocols who required marrow biopsy due to concern for cytopenia or myelodysplastic syndrome (MDS). To ensure assessment specifically for long term cytopenia only bone marrows after D+85 were included. For the oncoprint analysis, if a patient had multiple qualifying bone marrow samples, mutations were aggregated into a single representation. Similarly, if patients developed tMN at any point in their treatment course they were considered as having tMN for the sake of this analysis. Likelihood testing was performed using logistic regression for all patients with post-CAR cytopenic marrows using the top 5 most frequently identified gene mutations in the entire dataset. Determination of tMN diagnosis was made based on clinician diagnosis in the medical record and the minimum consensus between the ICC[4] and WHO version 5[5] guidelines for MDS as noted above. Definition of clonal cytopenia of indeterminate significance (CCUS) and idiopathic cytopenia of undetermined significance (ICUS) followed WHO version 5 consensus guidelines.

Flow Cytometry Analysis of CAR19 in Blood and Bone Marrow

Flow cytometric analysis of patient bone marrow and peripheral blood was performed as previously described[1,6,7]. Blood and bone marrow samples were collected as clinically indicated and were processed fresh and in parallel. Flow cytometry samples were collected in K2EDTA or sodium heparin containing tubes and processed immediately as previously described[7,8]. Briefly, peripheral blood mononuclear cells (PBMCs) were obtained from ~8 mL of fresh whole blood and isolated by density gradient centrifugation with Ficoll-Plague Plus (GE Healthcare). PBMCs were stained with fixable Live/Dead Aqua amine-reactive viability stain (Invitrogen, L-34965). Fc receptors were blocked with Human TruStain FcX (BioLegend, 422302) for 5 minutes to prevent non-specific antibody binding. Cells were then stained at room temperature with a fluorochrome-conjugated antibody panel[7]. Stained and fixed cells were acquired on a four-laser LSRII flow

cytometer (BD Biosciences; blue: 488-nm, violet: 405-nm, red: 640-nm and green: 532-nm lasers; 21 parameters). A minimum of 1 million cells were acquired unless limited by the total number of isolated cells. Gating for $CD4^+$ and $CD8^+$ CAR19 T-cells within viable $CD45^+$ cell population was performed using Cytobank software. Sample gating was performed by a team of expert research specialist who were blinded to the clinical status of individual patients. In addition to standard previously published flow cytometry methods a B-cell panel was developed to assess B cell differentiation stages in peripheral blood and bone marrow as depicted in the below table.

#	Antibody Color	Channel	Cat. Nr.
1	FITC CD3	B525	300440
2	PerCP5.5 CD8	B710	301032
3	PE CD19	G575	363004
4	BV785 CD45	V780	368528
5	BV605 CD27	V605	302830
6	APC Cy7 CD38	R780	303534
7	Alexa Flour 700 CD5	R710	300632
8	APC IgD	R670	348222
9	PE Cy7 CD10	G780	312214
10	BV711 CD4	V710	300558
12	Zombie Aqua (live/Dead)	V515	423102

Luminex protein analysis:

Luminex-based protein quantification was performed on the plasma fraction of bone marrow aspirates. Samples were run in duplicate, and mean protein levels were used for downstream analysis. Differences in protein expression between CAR T-cell treated patients and healthy controls were evaluated using two-sample t-tests with Bonferroni correction.

Single Cell RNA Sequencing Analysis

Single cell RNA data generation was performed on fresh bone marrow aspirate cells, after pre-processing to isolate live, non-red cells, using standard protocols (10x Genomics). A total of 25-30,000 reads per cell was targeted for each sample with variation dependent on total cells captured after processing. Single cell RNA sequencing analysis included 5' gene expression sequencing, TCR sequencing and BCR sequencing as previously described[7]. For alignment to the axi-cel vector a custom chromosome was inserted into the Cell Ranger human reference genome with sequence homology to axi-cel. The CD3 region of the vector was removed to enforce specificity and avoid cross homology to other BCRs. Specificity was confirmed using axi-cel product as a positive control and control healthy bone marrow as a negative control. Similar methods were used to map to the CAR22 vector however the EF1 transcriptional promoter was also removed due to overlap with the human genome. Specificity of sequence reads were confirmed on CAR22 product controls using pre-infusion human peripheral blood as a negative control for the reference. In the case of both axi-cel and CAR22 negative controls there were zero incorrectly mapped reads to the vector sequence.

Sequence processing and cell assignment: The Seurat algorithm was used for sequence processing after Cell Ranger alignment using default parameters. Individual sample data was merged and processed with SCT transformation as previously described[6,7]. Due to consistent processing and most samples being handled fresh after aspiration or blood draw no integration methods were used. Azimuth was used to define cell types with simplification as needed into cell groups. scRepertoire was used for TCR processing, TCR diversity estimates, and TCR assignment to individual cells again using default parameters[9]. Wilcoxon testing was used to define differences in tested variables. Propeller was used for global differential cell distribution analysis[10]. For hypothesis specific testing comparing CD4+ CAR T-cells and ratios of immature vs mature B-cells with smaller n-values per cell all cellular data was grouped, and a Fisher test was performed. For immature versus mature B-cell analysis, one CAR-treated patient with documented peripheral B-cell recovery by clinical flow cytometry was excluded. The Cell Ranger output summary was used to define predicted cells with product VDJ-B/Ig and individual differences in the log transformed values were compared using a Wilcoxon test.

For statistical testing between measures of T and B cell clonality where were measured on a per-sample basis a Wilcoxon test was used to define differences in sample populations. For global analysis of multiple cell lineage states the Propeller[10] algorithm was used. For comparison of a single lineage state (i.e. immature B-cells or CD4 T-cells) relative to all other lineages all available samples were grouped, and a Fisher test was performed. For measurement of differential RNA expression levels (such as testing for inflammatory enrichment) a pseudobulk differential expression was used merging samples derived from the same timepoint. The gene set enrichment analysis (GSEA)[11] toolkit was used to assign hallmark gene expression programs to differential expression patterns discovered in pseudobulk differential expression testing.

Analysis of tMN in HCT vs CAR treated patients:

The presence of tMN was assessed in n = 724 CAR patients as described previously[6]. Cumulative incidence for tMN was defined as a competing risk regression using the cmprsk package in R with death as a competing risk. For patients with multiple CAR-T infusions incidence was calculated from the time of the first infusion. tMN was defined by patients meeting the minimum criteria for tMN between the ICC[4] and WHO version 5[5] classification of myeloid neoplasms.

To assess a reasonable comparator population, we focused on the non-Hodgkin lymphoma (NHL) patient population from this study and compared to patients treated with only autologous stem cell transplant (HCT). For the HCT comparator arm we analyzed n = 1007 patients treated at Stanford (2006 – 2022). No attempt at comparing cumulative incidence was made due to multiple cell therapy infusions in most tMN CAR patients. Only patients developing MDS and AML were included for comparator analysis (excludes n = 2 CMML in the HCT group). Pre-treatment risk was determined by Revised International Prognostic Scoring System (IPSSR) at the time of diagnosis[12]. Comparison of mutational profiles was not attempted due to paucity of molecular data in the HCT group. Complex karyotype is defined as 3 or more chromosome alternations on cytogenetics[12,13]. Loss of chromosome 5 or chromosome 7 could be determined by either fluorescent in-situ hybridization (FISH) or standard karyotype. Death was defined as death from any cause. Relapse free survival was defined as tumor progression after first line therapy or death from any cause. Survival analysis was performed in R using the survival package and log-rank analysis.

Once defined the n = 29 post-HCT tMN and n = 17 post-CAR tMN were compared using Wilcoxon test for continuous variables and a Fisher test for categorical variables (TableOne package in R)

as previously described[1]. P-values are not corrected for multiple hypothesis testing due to the small number of variables assessed in each comparison. Clinical molecular marrow results were determined using clinical sequencing data from myeloid mutation panels and standard karyotype and FISH analysis for myeloid mutation testing. IPSSR was defined from marrow at diagnosis for each patient using complete blood count results from the nearest timepoint to the clinical marrow. PFS was defined as any progression of myeloid malignancy after treatment or death from any cause relative to the time of tMN diagnosis. OS was defined as the time to death from any cause after tMN diagnosis.

CAPP-seq

CAPP-seq assays were performed as previously described for targeted sequencing of 772 kb including 151 fully covered genes and 488 partially covered genes that are recurrently mutated in lymphoid neoplasms ("BLYM")[14,15], as well as the axi-cel retroviral construct; simultaneous tumor and effector profiling (STEP) analysis were performed as previously described[15]. A second smaller panel of 267 kb ("MRD") was additionally used for performing clonal tracing. Both panels contain 17 CH genes, 8 with full coverage of the coding region and 9 with partial coverage at mutation hotspot regions. Detailed processing steps are described elsewhere.

CH Variant Calling and Enrichment Analysis

FASTQ files were demultiplexed based on 8-bp dual sample barcodes and reads were mapped to a customized version of the human reference genome (hg19) augmented with the retroviral sequence for axi-cel using BWA-MEM2. Molecules were deduplicated with error-suppression using a custom pipeline as previously described[16]. Following this, somatic single nucleotide variants (SNV) and insertion-deletion variants (indels) were called using a custom variant algorithm optimized for cfDNA as previously described[16]. Callsets were further refined by removing variants that were detected in greater than 10% of samples in a separate control cohort. Variants that were detected in gnomAD with a minor allele frequency (MAF) exceeding a threshold of 0.015% were removed. This threshold was selected to ensure a 5% or lower probability of observing the allele at least once in our cohort by random chance.

Following variant calling, we computed the union of all call sets for each patient and monitored the variant allele frequency of all variants in all available samples. The resulting monitoring set was further refined by removing variants that were called in over 80% of patients in our cohort, filtering to remove variants with less than 5 supporting reads, and filtering by ANNOVAR functional annotation. Specifically, we excluded variants with the ncRNA_intronic, ncRNA_exonic, intergenic, intronic, synonymous, upstream, downstream, UTR5, and UTR3 annotations. For our enrichment analysis, we further restricted the monitoring set to include only protein coding genes. Pre-infusion CH was defined as any CH in 17 targeted CH genes from pre-infusion PBMC samples. Likely global CH analysis (used for doubling time and Figure 5E) was defined as pre-infusion CH as well as CH mutations detected in day greater than or equal to 28 in non-progressors

To enable identification of emergent or clonally selected non-tumor alterations in responders, we assessed cases with paired peripheral blood leukocyte (PBL) samples available at pre-CAR T infusion and plasma or PBL samples available at timepoints following sustained minimal residual disease (MRD) negativity. To control for differences in allele frequency between samples, we ranked the clonal hierarchy of variants as follows: In a set of n variants [mut_1, mut_2, …, mut_n], we identified the allele fractions in the earliest timepoint samples as [$AF1_{mut1}$, $AF1_{mut2}$,

… , $AF1_{mutn}$] and the allele fractions in the last timepoint sample as [AF2mut1, $AF2_{mut1}$, $AF2_{mut2}$, … , $AF2_{mutn}$]. Within each sample, we then defined a distribution across all variants representing the selection of each variant by calculating:

$$S_i = log_{10} \frac{AF2_{mut_i}}{AF1_{mut_i}}$$

for each variant. This value was log-transformed to create an approximately normal distribution.

For each case, all SNVs and indels were then assigned a z-score based on this distribution:

$$z_i = \frac{S_i - \mu_S}{\sigma_S}$$

This Z-score thus represents the selective pressure placed on each variant in each given case, with variants under positive selection receiving high scores and those under negative selection receiving low scores. We finally assessed the recurrent selective pressure on genes of interest by assessing the set of Z-score for alterations in a gene of interest compared to all other alterations using a Wilcoxon rank-sum test.

Analysis of Clonal Hematopoiesis Frequency and Mutational Burden in Treatment Naive and Pre-CAR-T Cohorts

To evaluate the frequency of mutations in genes associated with clonal hematopoiesis (CH) at the pre-infusion timepoint, we first identified 101 LBCL patients with available pre-CAR-T peripheral blood leukocyte (PBL) samples and 124 treatment-naive LBCL patients with available PBL samples from a separate cohort. We then matched cases based on age and median sequencing depth to identify 101 treatment-naive and 101 pre-CAR-T infusion samples for analysis. Using the SNV and indel call sets from these samples, we computed the frequency of mutations in a set of 17 genes associated with (CH). Variants were filtered as previously described in the CH Variant Calling section. Variant frequency was computed independently for VAF greater than or equal to 2% and less than 2%, consistent with the clinical definition of CH. An uncorrected Fisher test was performed to compare relative fraction of CH mutations in genes with >= 3 mutations in the pre-CAR group.

Analysis of immune reconstitution in patients with pre-existing CH mutations

Immune reconstitution data was collected in the same manner as immune reconstitution after CAR and HCT described above, however data cutoff was set at day 180. Patients were included if: 1) they treatment of LBCL with CAR T-cell therapy, 2) they had pre-infusion CH in PBL samples as defined above and 3) they had no evidence of disease relapse at D+180 to avoid confounding from subsequent chemotherapies. Immune reconstitution testing was measured by longitudinal analysis of day 28- day 180 serial CBC samples for ANC, ALC, platelets, and hemoglobin using the same linear mixed effects modeling as described above. For multivariate analysis included variables were age, sex, and CAR HEMATOTOX score. Like above timepoints were treated as categorical variables and interaction terms between time and each multivariate parameter were included in the modeling.

Single Cell DNA Sequencing Analysis

Generation of single cell DNA sequencing data was performed according to manufacturer protocols using viably preserved bone marrow aspirate cells (Mission Bio). A custom single cell panel was designed using the Mission Bio Myeloid Clonal Evolution amplicon panel[17] as a background with additional custom amplicons focused on specific CH mutations targeted against known clinical mutations. To detect axi-cel an 11-amplicon custom panel that tiled the axi-cel vector between the long terminal repeats (LTRs) was generated with forward and reverse primers that excluded human sequence homology. A standard 45-gene antibody (Total-seq D, BioLegend) directed against cell-surface antigens was used for single cell protein immune profiling.

scDNA data alignment was performed using the Tapestri Pipeline to hg19 with the axi-cel vector added as a custom chromosome. Single cell DNA analysis was performed using the Mission Bio Mosaic pipeline using default parameters and center log ratio normalization of protein sequencing reads. Cell identities were determined by nearest neighbor clustering results combined with analysis of dominant protein expression per cluster. Axi-cel vector was detected using copy number variation clustering using the Mosaic pipeline.

Individual gene mutations were accepted if they were in the coding region and caused a change in the protein sequence or if they were in a splicing region and annotated as likely pathogenic. Mutations were grouped into individual clones, with each clone defined by a unique combination of gene alterations in a cell group. The compass algorithm was used for clonal phylogenetic tracing[18]. Cell lineages were broadly defined manually in Omiq based on cell surface marker expression from an expert pathologist based on cell surface markers from DNA-antibody sequencing as described in Figure S7. A Fisher test was used to determine abundance differences in DDR gene mutations between NK cells relative to all other lymphocytes by comparing the total incidence of DDR and age-related mutations in both populations without respect to lymphocyte sub-populations (ie CD4+ and CD8+ T-cells).

In five patients axi-cel DNA was discovered within cells containing *DNMT3A* and *TET2* mutations (however n > 1 cell in only 3 patients). In these cases, enrichment analysis was performed by comparing the total number of axi-cel-positive mutant T-cells relative to the distribution of the mutation in as a percent of all T-cells.

Part II Supplementary Figures

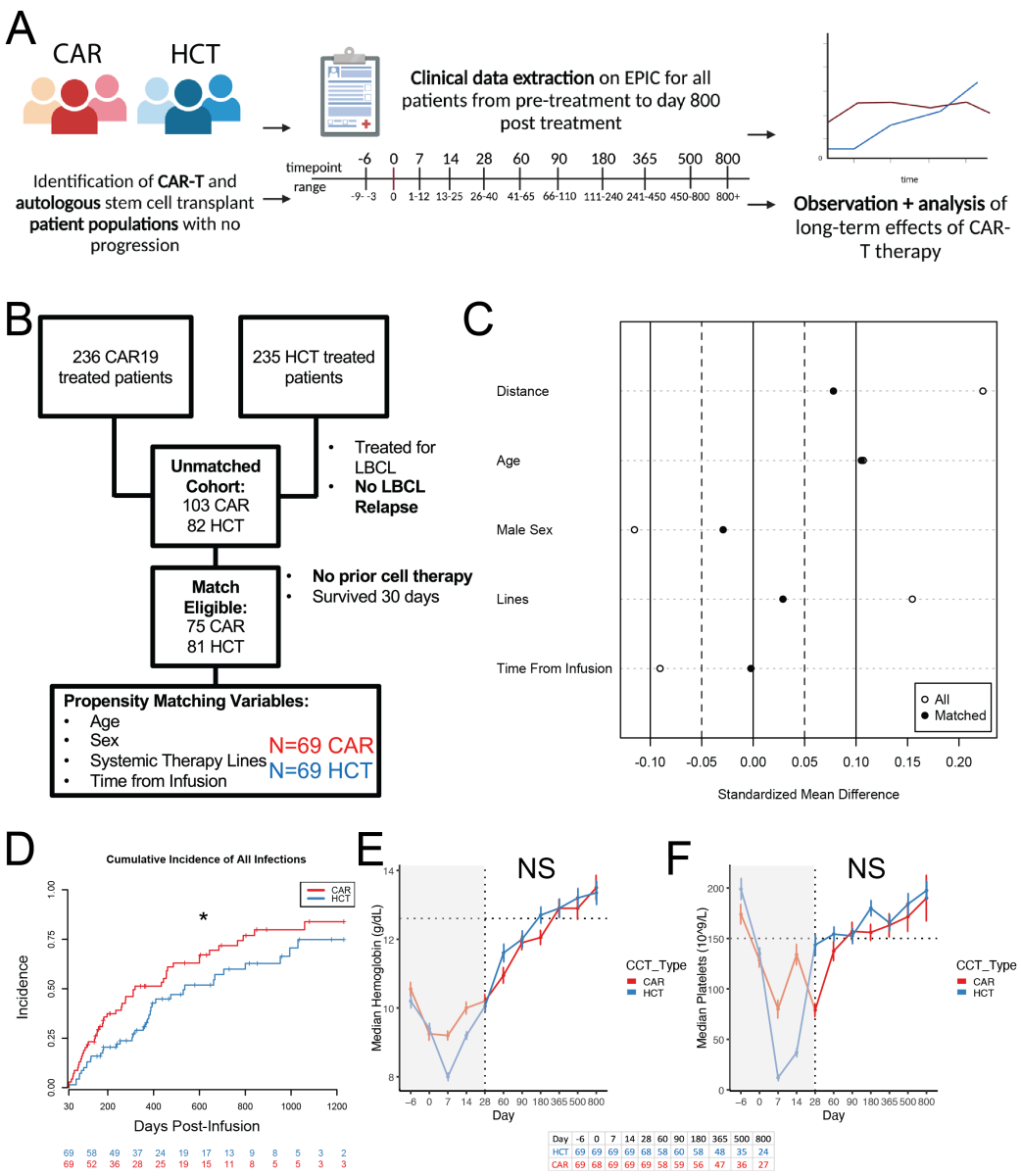

Figure S1: Increased infection and reduced immune reconstitution in CAR vs HCT treated patients. A) Overview of data collection windows. **B)** Consort diagram of non-relapsed HCT and CAR treated patients were propensity matched to compare infection and immune reconstitution. **C)** Standardized mean differences for matched variables in eligible cohorts. Vertical dotted lines represent acceptable balance thresholds. **D)** Cumulative incidence of all-grade infections post-infusion in matched CAR and HCT cohorts. CAR-treated patients had a modest but statistically significant increase in infection rates. *p < 0.05, competing risk regression. **E-F)** Longitudinal recovery of hemoglobin (D) and platelet counts (E) in CAR- vs HCT-treated patients. No significant differences were observed (NS, not significant). CAR, chimeric antigen receptor; HCT, hematopoietic cell transplantation; CONSORT, Consolidated Standards of Reporting Trials.

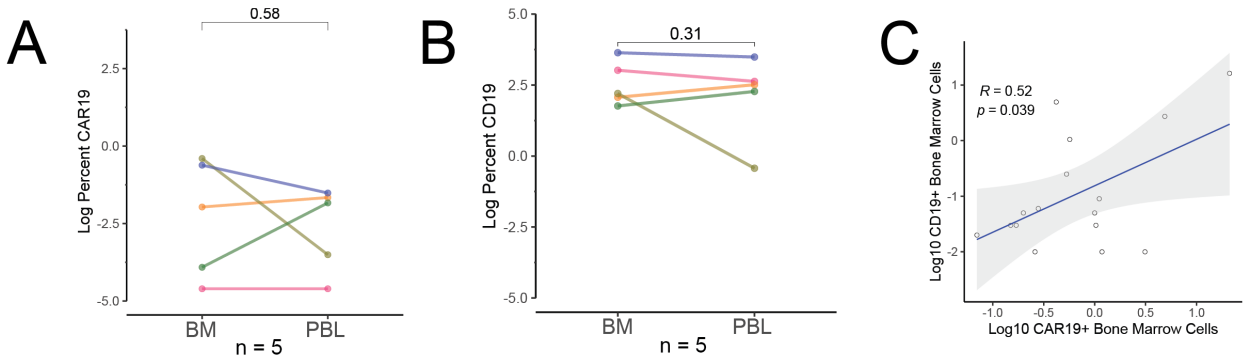

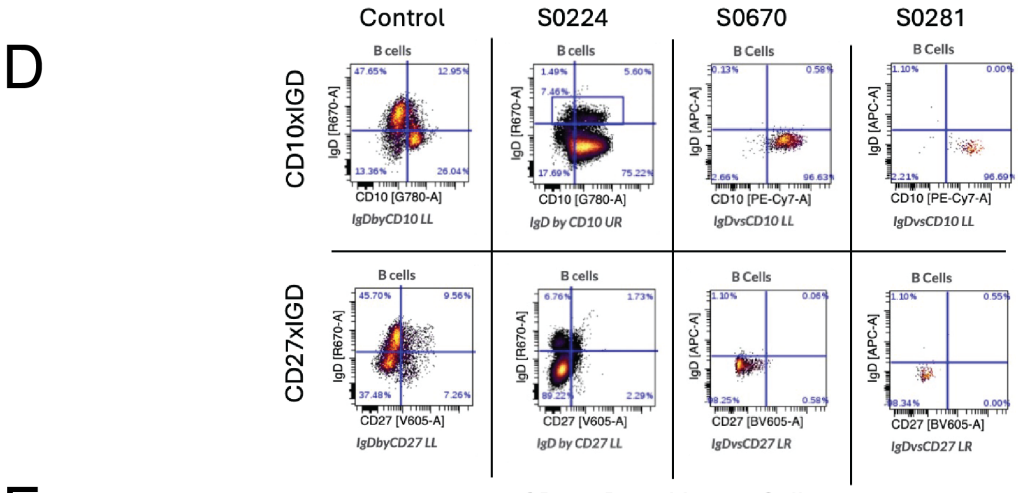

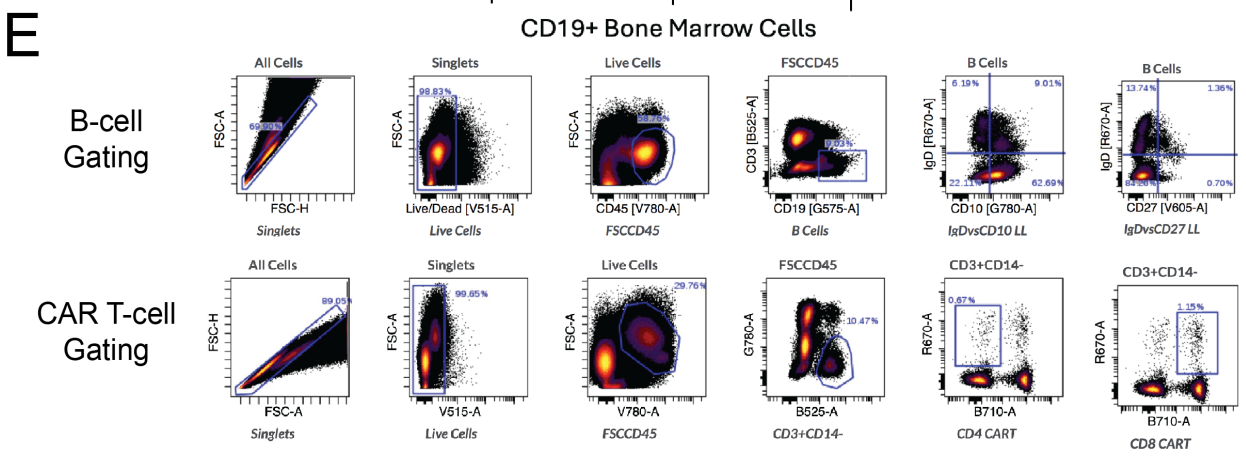

F

Gene	1	2	3	4	5	6	7	8	9	10	11	12	P	Corrected
IL4													****	*
PDGFAA													****	*
PDGF-AA/AB													****	*
CCL7													****	*
IL13													****	*
SCD40L													***	NS
CX3CL1													***	NS
IL17F													*	NS
VEGF													*	NS
IL12P70													*	NS
IL22													*	NS
IP-10/CXCL10													*	NS
MIP1A/CCL3													*	NS

Figure S2: Increased inflammation and clonal T-cell infiltration in post-CAR cytopenic marrows. A-B) CAR19 (A) and CD19 (B) expression levels in paired BM and PBL from five healthy donors. No significant difference was observed between compartments. **C)** Weak positive correlation between $CAR19^+$ T-cell frequency and $CD19^+$ B-cell levels in bone marrow samples from post-CAR cytopenic patients ($R = 0.52$, $p = 0.039$). **D)** Representative flow cytometry plots of CD19-gated marrow cells demonstrating residual $CD19^+CD10^+CD27^-$ B-cell progenitors in bone marrow of post-CAR patients compared to healthy controls. **E)** Representative B-cell (top panel) and CAR (bottom panel) gating. **F)** Heatmap of cytokine and growth factor expression in $CD19^+$ marrow compartments across 12 post-CAR patients. IL-4, PDGF-AA/BB, and CCL7 are significantly downregulated (Bonferroni-adjusted p-values shown; $^*p < 0.05$, $^{**}p < 0.01$, $^{***}p < 0.001$, $^{****}p < 0.0001$). BM, bone marrow; PBL, peripheral blood leukocyte; CAR, chimeric antigen receptor; PDGF, platelet-derived growth factor.

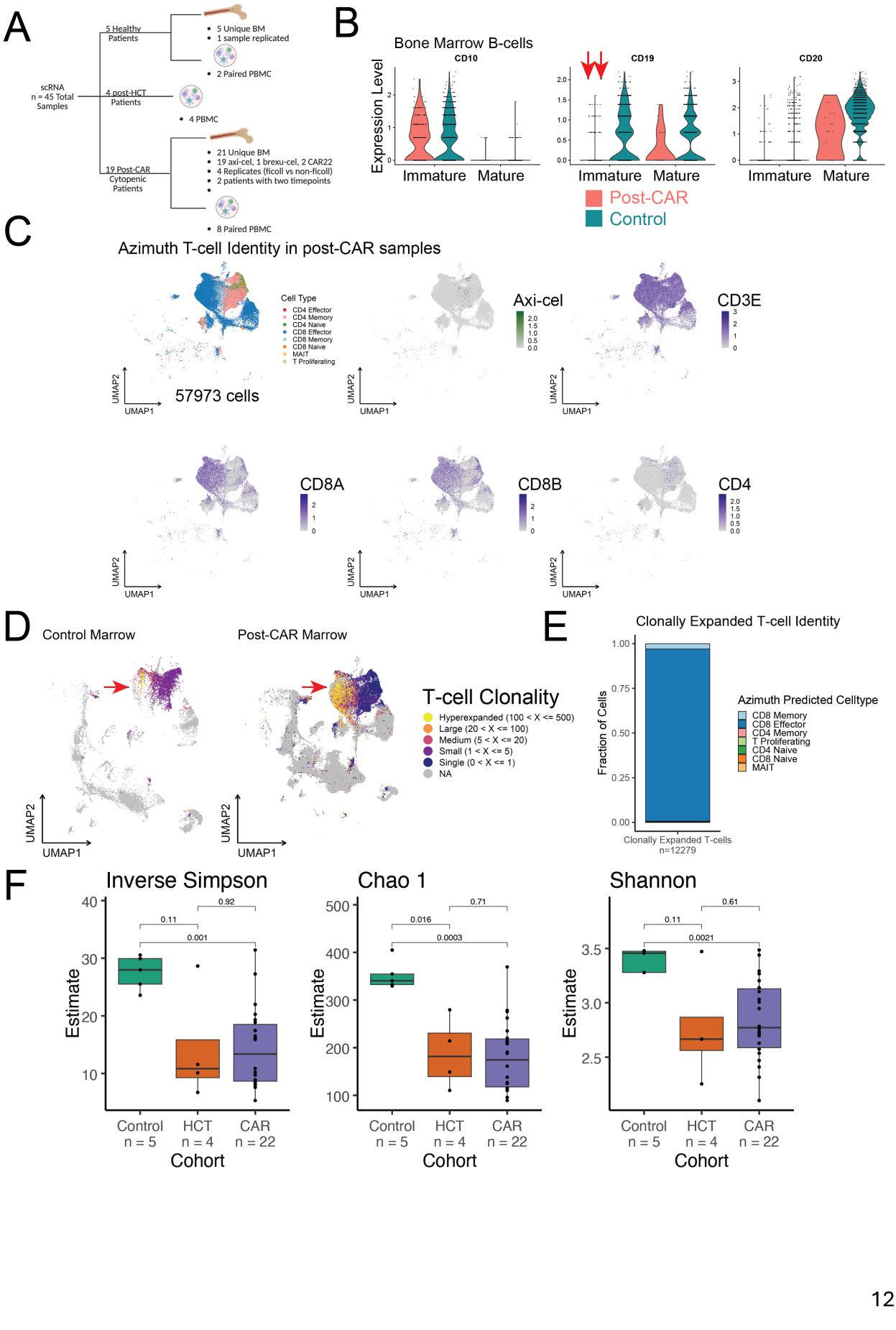
A
scRNA
n = 45 Total
Samples
5 Healthy
Patients
4 post-HCT
Patients
19 Post-CAR
Cytopenic
Patients
5 Unique BM
1 sample replicated
2 Paired PBMC
4 PBMC
21 Unique BM
19 axi-cel, 1 brexu-cel, 2 CAR22
4 Replicates (ficoll vs non-ficoll)
2 patients with two timepoints
8 Paired PBMC
B
Bone Marrow B-cells
CD10
CD19
CD20
Expression Level
Immature
Mature
Post-CAR
Control
C
Azimuth T-cell Identity in post-CAR samples
Cell Type
CD4 Effector
CD4 Memory
CD4 Naive
CD8 Effector
CD8 Memory
CD8 Naive
MAIT
T Proliferating
57973 cells
Axi-cel
CD3E
CD8A
CD8B
CD4
UMAP1
UMAP2
D
Control Marrow
Post-CAR Marrow
T-cell Clonality
Hyperexpanded (100 < X <= 500)
Large (20 < X <= 100)
Medium (5 < X <= 20)
Small (1 < X <= 5)
Single (0 < X <= 1)
NA
E
Clonally Expanded T-cell Identity
Fraction of Cells
Clonally Expanded T-cells
n=12279
Azimuth Predicted Celltype
CD8 Memory
CD8 Effector
CD4 Memory
T Proliferating
CD4 Naive
CD8 Naive
MAIT
F
Inverse Simpson
Chao 1
Shannon
Estimate
0.11
0.92
0.001
0.016
0.71
0.0003
0.0021
0.61
Control
n = 5
HCT
n = 4
CAR
n = 22
Cohort

Figure S3: A) Overview of scRNA samples. **B)** Expression of CD10, CD19, and CD20 in bone marrow B-cell populations from post-CAR cytopenic patients and healthy controls. Immature B cells in post-CAR samples are CD10+ and CD20-, consistent with a progenitor phenotype. **C)** UMAP projections of T cells in post-CAR samples with Azimuth-defined cell identities. Axi-cel transcript is detected in rare cells, predominantly within CD4+ T-cell subsets. CD22 CAR was detected by transcript but did not pass filtering thresholds in post-CAR22 samples. **D)** T-cell receptor clonality in bone marrow and peripheral blood from post-CAR patients vs healthy controls. Expanded clones are present in post-CAR but not in control marrows. **E)** Clonally expanded T cells in post-CAR samples are almost exclusively predicted as CD8+ effector cells by Azimuth classification. **F)** T-cell diversity metrics (Inverse Simpson, Chao1, Shannon) reveal reduced diversity and increased clonality in CAR-treated patients relative to healthy controls. Post-HCT peripheral blood samples demonstrate similar reductions, suggesting a general effect of cytotoxic therapy and immune reconstitution rather than CAR-specific selection. CAR, chimeric antigen receptor; HCT, hematopoietic cell transplantation; PBL, peripheral blood lymphocyte; UMAP, uniform manifold approximation and projection.

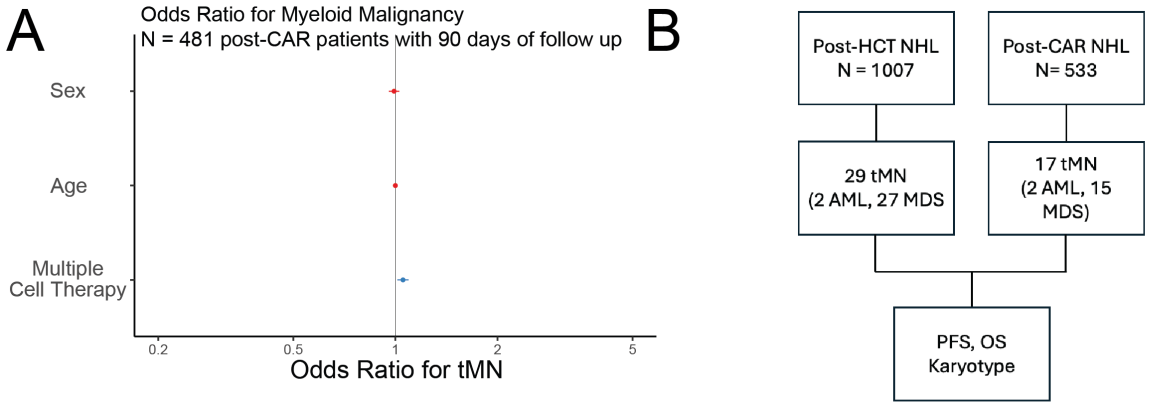
A
Odds Ratio for Myeloid Malignancy
N = 481 post-CAR patients with 90 days of follow up
Sex
Age
Multiple
Cell Therapy
0.2
0.5
1
2
5
Odds Ratio for tMN
B
Post-HCT NHL
N = 1007
Post-CAR NHL
N= 533
29 tMN
(2 AML, 27 MDS
17 tMN
(2 AML, 15
MDS)
PFS, OS
Karyotype

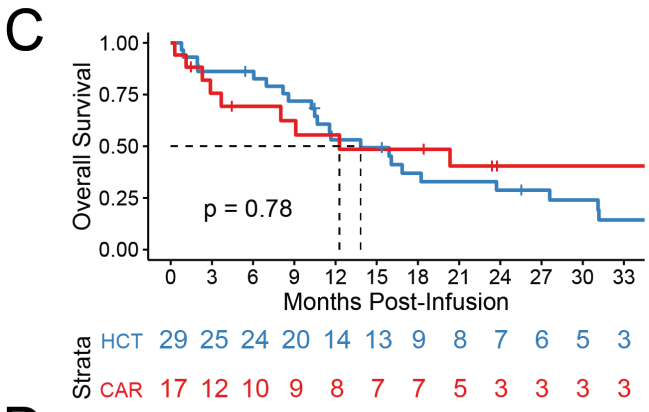
C
Overall Survival
1.00
0.75
0.50
0.25
0.00
p = 0.78
0 3 6 9 12 15 18 21 24 27 30 33
Months Post-Infusion
Strata
HCT 29 25 24 20 14 13 9 8 7 6 5 3
CAR 17 12 10 9 8 7 7 5 3 3 3 3

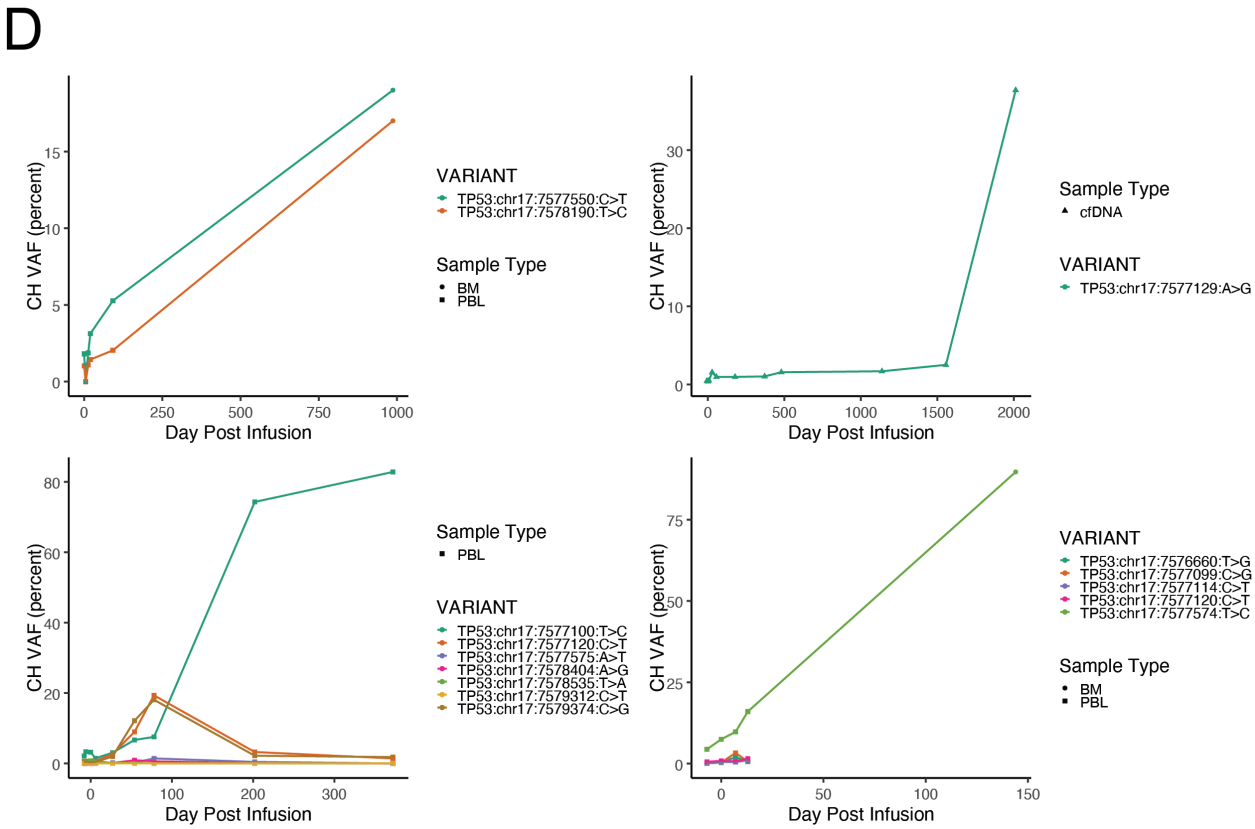
D
CH VAF (percent)
Day Post Infusion
VARIANT
TP53:chr17:7577550:C>T
TP53:chr17:7578190:T>C
Sample Type
BM
PBL
CH VAF (percent)
Day Post Infusion
Sample Type
cfDNA
VARIANT
TP53:chr17:7577129:A>G
CH VAF (percent)
Day Post Infusion
Sample Type
PBL
VARIANT
TP53:chr17:7577100:T>C
TP53:chr17:7577120:C>T
TP53:chr17:7577575:A>T
TP53:chr17:7578404:A>G
TP53:chr17:7578535:T>A
TP53:chr17:7579312:C>T
TP53:chr17:7579374:C>G
CH VAF (percent)
Day Post Infusion
VARIANT
TP53:chr17:7576660:T>G
TP53:chr17:7577099:C>G
TP53:chr17:7577114:C>T
TP53:chr17:7577120:C>T
TP53:chr17:7577574:T>C
Sample Type
BM
PBL

Figure S4: The majority of post-CAR tMN occurs through expansion of pre-existing TP53 clonal hematopoiesis. A) Odds ratios for development of tMN among 481 post-CAR patients with ≥90 days of follow-up. Receipt of multiple cellular therapies (e.g., CAR after HCT or a second CAR infusion) was significantly associated with increased tMN risk. **B)** CONSORT diagram comparing post-HCT and post-CAR tMN cases. A total of 29 post-HCT and 17 post-CAR tMN cases were identified, with comparable rates of AML and MDS. **C)** Overall survival after tMN diagnosis was not significantly different between post-CAR and post-HCT cohorts (log-rank p = 0.78). **D)** Representative VAF trajectories illustrating two dominant patterns of TP53 clonal evolution: (1) expansion of multi-hit TP53 mutations detectable at peri-infusion; and (2) expansion of mono-allelic TP53 mutations that undergo LOH after infusion. These clonal dynamics suggest both early seeding and therapy-driven transformation. CH, clonal hematopoiesis; tMN, therapy-related myeloid neoplasm; CAR, chimeric antigen receptor; HCT, hematopoietic cell transplantation; OS, overall survival.

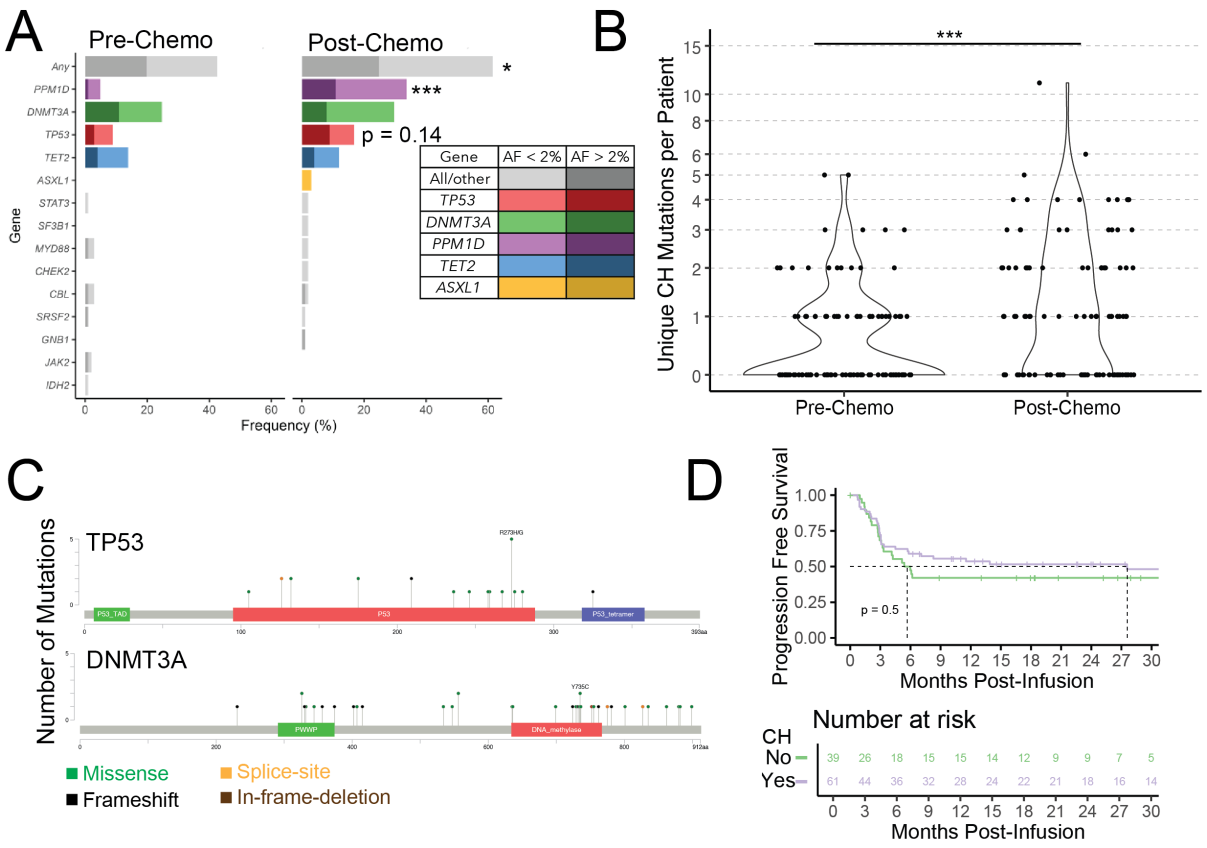

Figure S5. Characteristics of CH before and after chemotherapy. A-B) In a matched analysis of 101 pre-treatment and 101 post-chemotherapy samples controlled for age and sequencing depth, CH frequency and per-patient CH burden were significantly elevated post-chemotherapy (main figure is an unmatched analysis). **C)** Pre-infusion functional mutations in DNMT3A cluster in the DNA methylation and PWWP domains, and in TP53 within the DNA-binding domain, consistent with canonical pathogenic variants. **D)** Presence of pre-infusion CH is not associated with inferior PFS following CAR T-cell therapy. CH, clonal hematopoiesis; VAF, variant allele frequency; PBL, peripheral blood lymphocyte; TMB, tumor mutational burden; PFS, progression-free survival.

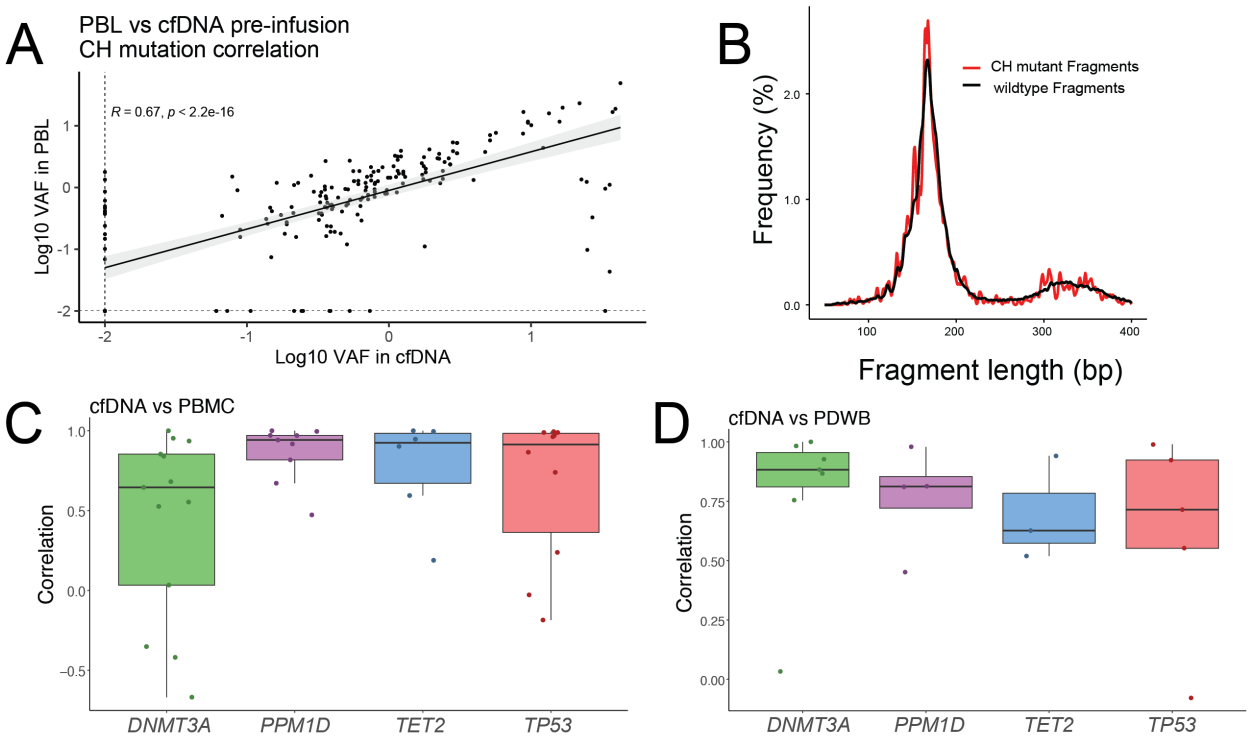

Figure S6: CH mutations are reliably measurable in cfDNA and expand post-CAR T-cell therapy. A) Correlation of CH VAF in pre-infusion paired cfDNA and PBL samples, demonstrating strong agreement ($R^2 = 0.83$). **B)** Fragment length distribution of cfDNA molecules containing CH mutations compared to wild-type sequences. Both distributions overlap, supporting hematopoietic origin of CH fragments. Unlike tumor-derived cfDNA, CH fragments do not exhibit shorter fragment lengths. **C-D)** Comparison of cfDNA CH VAF with matched PBMC (C) and PDWB (D) confirms consistent clonal tracking across sample types. cfDNA, cell-free DNA; CH, clonal hematopoiesis; PBL, peripheral blood lymphocyte; PBMC, peripheral blood mononuclear cell; PDWB, plasma-depleted whole blood; VAF, variant allele frequency.

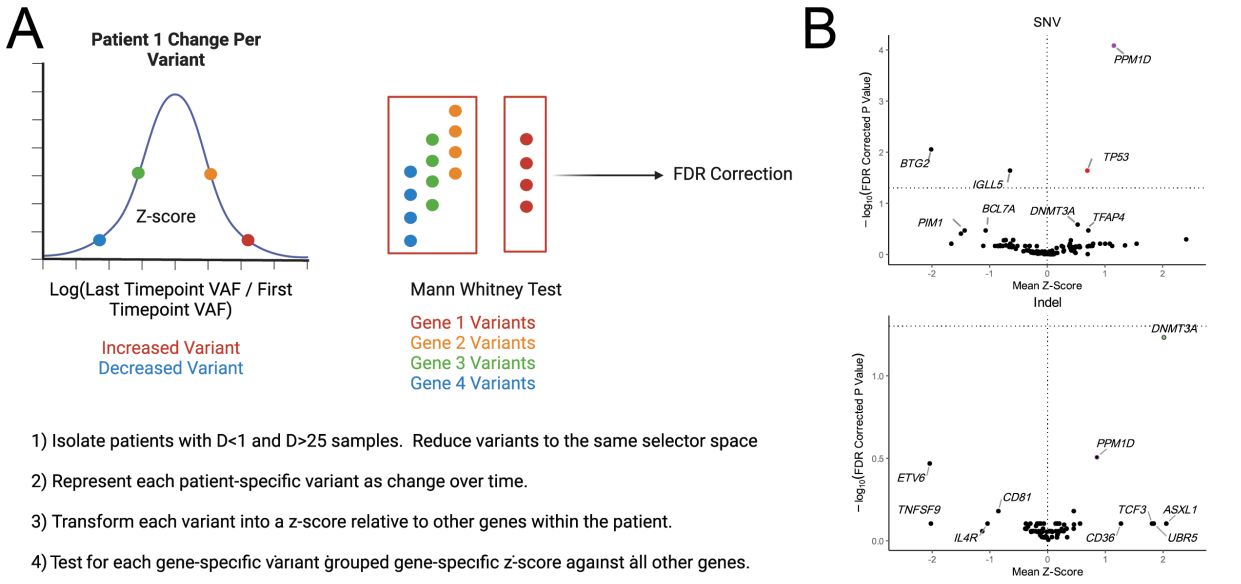

1) Isolate patients with D<1 and D>25 samples. Reduce variants to the same selector space

2) Represent each patient-specific variant as change over time.

3) Transform each variant into a z-score relative to other genes within the patient.

4) Test for each gene-specific variant grouped gene-specific z-score against all other genes.

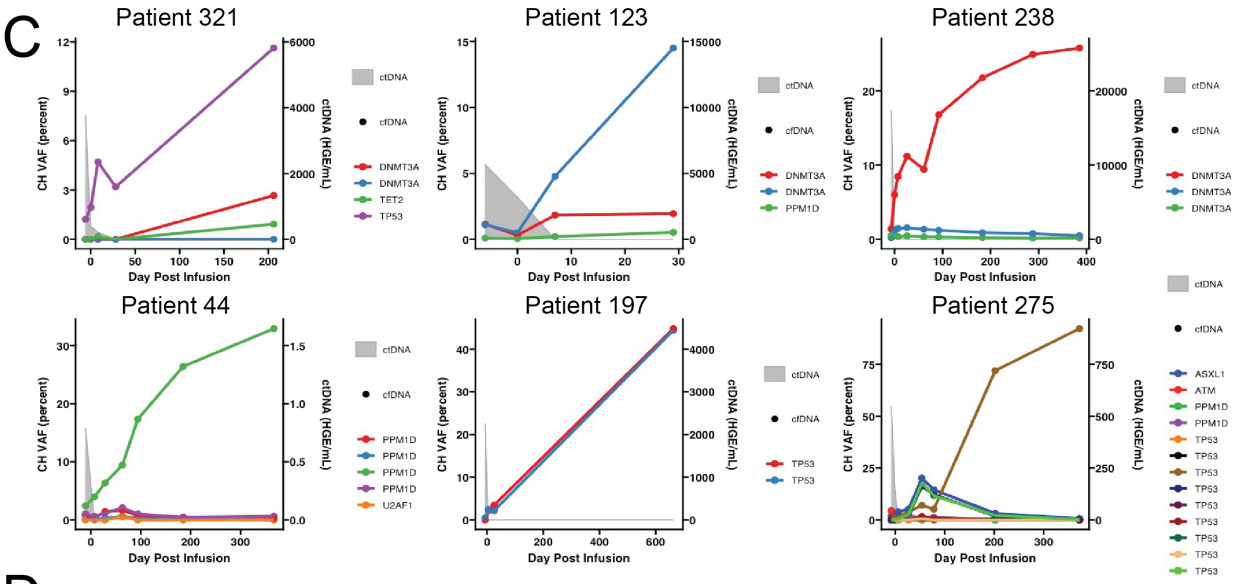

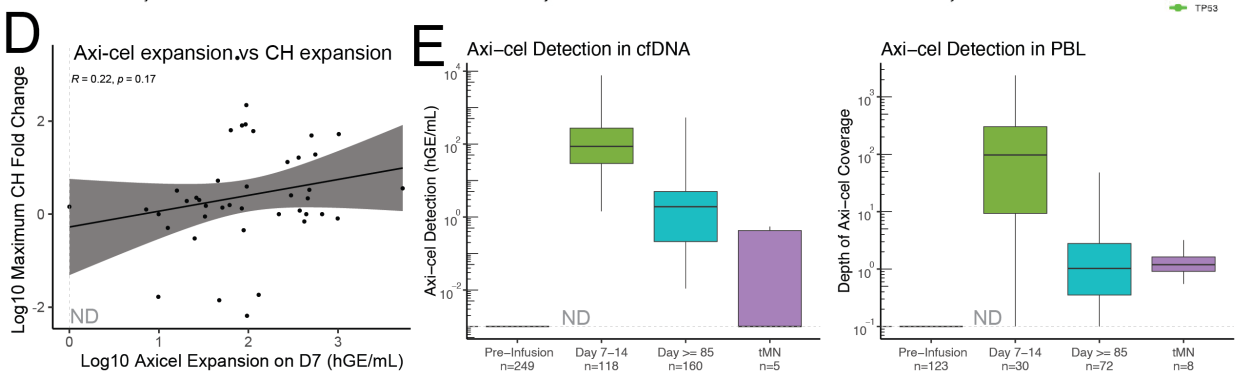

Figure S7: CH expands after CAR infusion, but CAR is not present in tMN. A) Schematic of the statistical framework used to evaluate post-infusion clonal expansion in patients without disease progression. Mutation-level changes in VAF between first and last timepoints were normalized as z-scores, and gene-specific enrichment was tested using Mann–Whitney U with FDR correction. **B)** Volcano plots displaying gene-level enrichment of SNVs (top) and indels (bottom) in post-infusion versus pre-infusion cfDNA from non-progressing patients. *TP53*, *PPM1D*, and *DNMT3A* are significantly enriched (FDR < 0.05), consistent with post-infusion CH expansion. **C)** Representative plots of CH expansion over time compared to rapid clearance in ctDNA. **D)** Axi-cel expansion on day 7 was not significantly associated with the degree of CH expansion across 44 evaluable patients. **E)** Axi-cel sequences were not enriched in cfDNA or PBL) samples from patients who developed tMN, suggesting absence of CAR integration in tMN clones. CH, clonal hematopoiesis; tMN, therapy-related myeloid neoplasm; cfDNA, cell-free DNA; PBL, peripheral blood lymphocyte; SNV, single nucleotide variant; VAF, variant allele frequency.

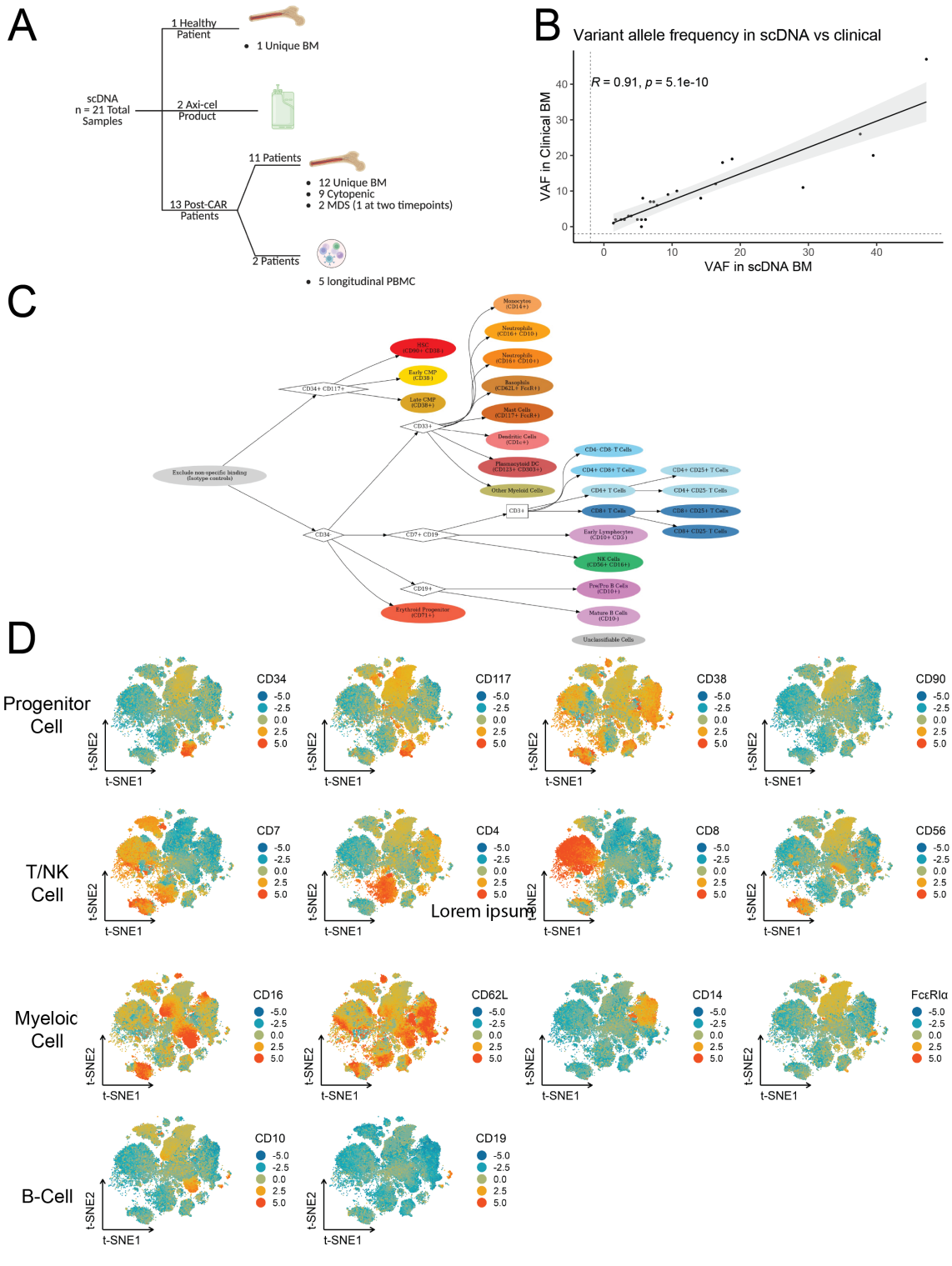
A
1 Healthy Patient
1 Unique BM
scDNA n = 21 Total Samples
2 Axi-cel Product
11 Patients
12 Unique BM
9 Cytopenic
2 MDS (1 at two timepoints)
13 Post-CAR Patients
2 Patients
5 longitudinal PBMC
B
Variant allele frequency in scDNA vs clinical
R = 0.91, p = 5.1e-10
VAF in Clinical BM
VAF in scDNA BM
C
D
Progenitor Cell
T/NK Cell
Myeloic Cell
B-Cell
CD34
CD117
CD38
CD90
CD7
CD4
CD8
CD56
CD16
CD62L
CD14
FcεRIα
CD10
CD19
t-SNE1
t-SNE2
Lorem ipsum

Figure S8: Single cell DNA sequencing defines post-CAR CH mutation burden in a cell lineage specific manner. A) Overview of scDNA sample collection. B) Variant allele fractions defined in scDNA-sequencing are strongly correlated with VAFs noted in clinical sequencing data detecting the same variant. **C)** Cell lineage assignment strategy using cell surface antibody profiles visualized and gated in Omiq. Lineage calls were based on a pre-defined marker-based algorithm and grouped by progenitor, lymphoid, myeloid, and B-cell categories. **D)** tSNE plots of DAb-seq marker expression across lineages confirm expected surface marker patterns for progenitor, T/NK, myeloid, and B-cell populations. scDNA-seq, single-cell DNA sequencing; VAF, variant allele frequency; CH, clonal hematopoiesis; NK, natural killer; DDR, DNA damage response; t-SNE, t-Distributed Stochastic Neighbor Embedding.

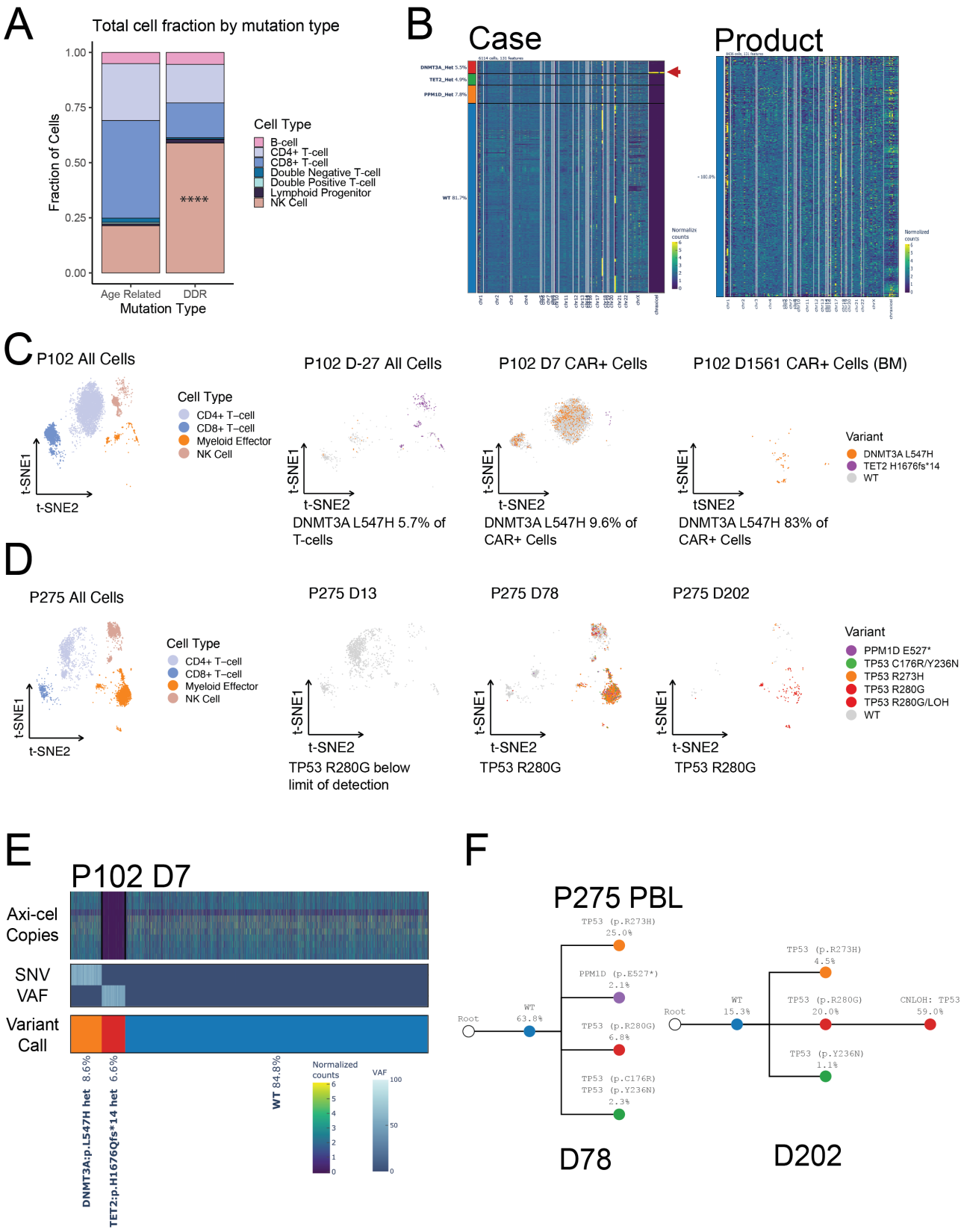
A
Total cell fraction by mutation type
Fraction of Cells
1.00
0.75
0.50
0.25
0.00
****
Age Related
DDR
Mutation Type
Cell Type
B-cell
CD4+ T-cell
CD8+ T-cell
Double Negative T-cell
Double Positive T-cell
Lymphoid Progenitor
NK Cell
B
Case
Product
DNMT3A_Het 5.5%
TET2_Het 4.9%
PPM1D_Het 7.8%
WT 81.7%
Normalized counts
C
P102 All Cells
t-SNE1
t-SNE2
Cell Type
CD4+ T–cell
CD8+ T–cell
Myeloid Effector
NK Cell
P102 D-27 All Cells
DNMT3A L547H 5.7% of T-cells
P102 D7 CAR+ Cells
DNMT3A L547H 9.6% of CAR+ Cells
P102 D1561 CAR+ Cells (BM)
tSNE2
DNMT3A L547H 83% of CAR+ Cells
Variant
DNMT3A L547H
TET2 H1676fs*14
WT
D
P275 All Cells
Cell Type
CD4+ T–cell
CD8+ T–cell
Myeloid Effector
NK Cell
P275 D13
TP53 R280G below limit of detection
P275 D78
TP53 R280G
P275 D202
TP53 R280G
Variant
PPM1D E527*
TP53 C176R/Y236N
TP53 R273H
TP53 R280G
TP53 R280G/LOH
WT
E
P102 D7
Axi-cel Copies
SNV VAF
Variant Call
DNMT3A:p.L547H het 8.6%
TET2:p.H1676Qfs*14 het 6.6%
WT 84.8%
Normalized counts
VAF
F
P275 PBL
Root
WT 63.8%
TP53 (p.R273H) 25.0%
PPM1D (p.E527*) 2.1%
TP53 (p.R280G) 6.8%
TP53 (p.C176R) TP53 (p.Y236N) 2.3%
D78
Root
WT 15.3%
TP53 (p.R273H) 4.5%
TP53 (p.R280G) 20.0%
CNLOH: TP53 59.0%
TP53 (p.Y236N) 1.1%
D202

Figure S9: Variable CAR integration and clonal competition revealed by scDNA-seq. **A)** In the lymphoid compartment DDR gene mutations are proportionately increased in NK cell populations indicating that DDR gene mutations persistent in hematopoietic stem cells and T-cells are spared possibly due to extramedullary proliferation. **B)** Targeted amplicon sequencing identifies axi-cel vector integration in post-CAR cytopenic bone marrow and in manufactured product samples. CAR+ cells are highly distinguishable and, in some cases, co-occur with CH mutations. **C)** Clonal tracing of patient 102 shows progressive expansion of a DNMT3A L547H clone from 5.7% of T cells at D-27 to 83% of CAR^+ bone marrow T cells at day 1561 indicating selection of the CAR+CH+ cell population **D)** Serial samples from patient 275 demonstrating *TP53* clonal competition during tMN development. **E)** In Patient 102, axi-cel preferentially integrates into a *DNMT3A*-mutant clone, while a coexisting *TET2*-mutant clone is excluded, consistent with lineage restriction of the *TET2* mutation. **F)** In Patient 275, serial PBL profiling on days 78 and 202 reveals clonal competition between multiple *TP53* variants. The TP53 R280G clone ultimately dominates following a presumed LOH event, consistent with myeloid transformation. Minimal *TP53* mutation burden was observed prior to CAR T-cell infusion. CAR, chimeric antigen receptor; scDNA-seq, single-cell DNA sequencing; LOH, loss of heterozygosity, BM, bone marrow; PBL, peripheral blood leukocytes; tMN, treatment-related myeloid neoplasm; t-SNE, t-Distributed Stochastic Neighbor Embedding.

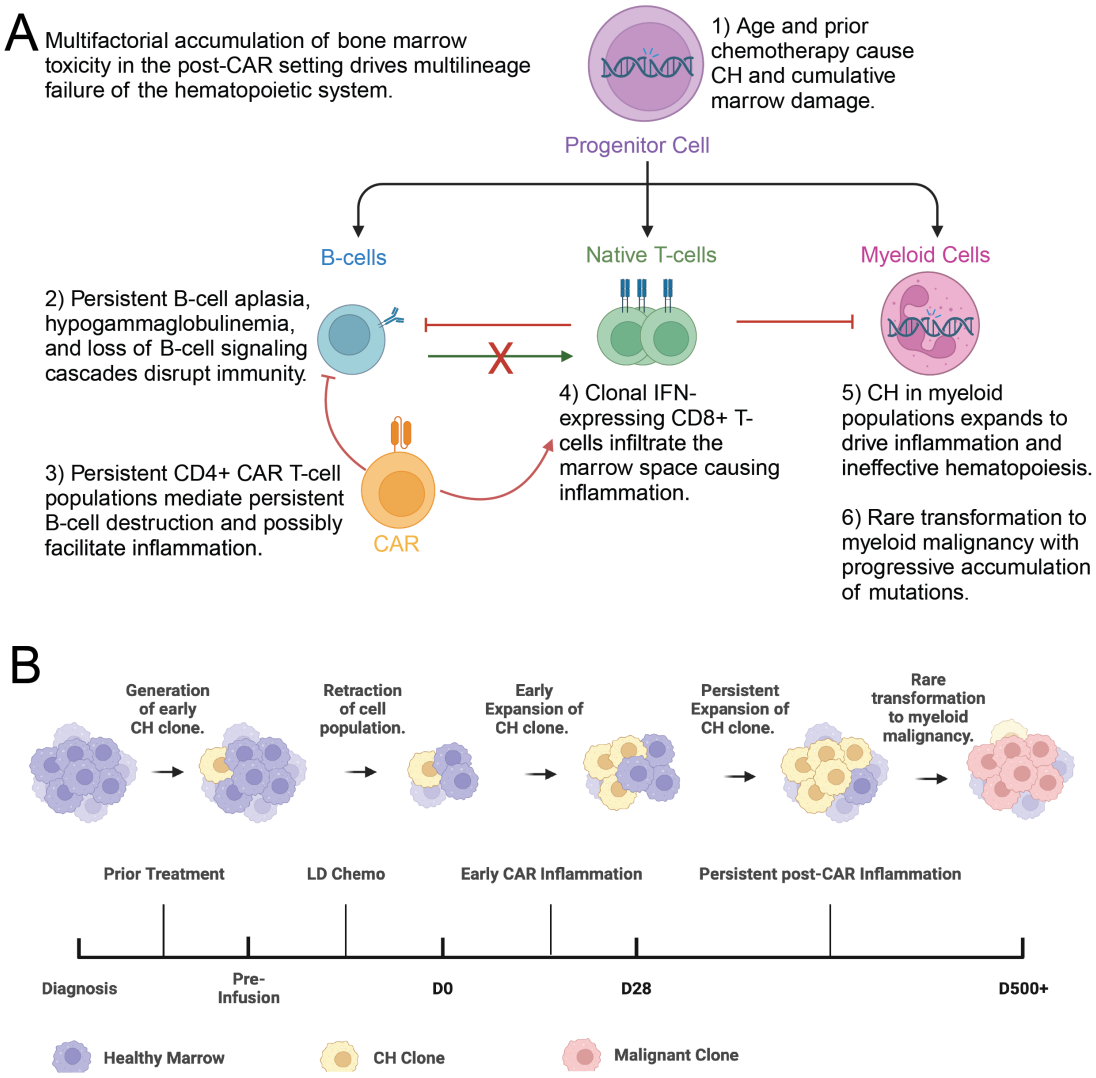

Figure S10: Model of CAR impact on the hematopoietic system. A) Schematic of post-CAR mechanisms leading to cytopenia, CH expansion, and post-CAR hematologic neoplasm. Post-CAR hematologic toxicity is likely highly complex involving multifactorial mechanisms that range from pre-infusion DNA damage causing direct toxicity to progenitor cell populations, to persistence of the CAR T-cell itself. In this publication we note major toxicities include 1) *a priori* DNA damage, 2) persistent B-cell aplasia coupled to persistent B-cell production and subsequent destruction, 3) persistent CAR T-cells, 4) clonal native non-CAR T-cells which express IFN gene programs, 5) expanding CH mutations in the myeloid cell line which is known to drive inflammation and ineffective hematopoiesis and 6) rare transformation of CH into tMN. The sum of this data indicates an inflammatory environment that impacts all major cell lineages and provides explanation for the persistent immune suppression and high rates of infection typically seen in the post-CAR environment. **B)** Timeline model of marrow injury and clonal evolution in the post-CAR setting. Early CH clones undergo retraction with conditioning chemotherapy, followed by re-expansion under inflammatory pressure from CAR therapy. Over time, persistent inflammation fosters selective outgrowth of DDR-mutated clones, contributing to marrow failure and rare progression to tMN. CH, clonal hematopoiesis; CAR, chimeric antigen receptor; tMN, therapy-related myeloid neoplasm.

Part III: Supplementary Tables

Variable	HCT	CAR	P-value
Age Mean (SD)	59.4 (10.7)	60.8 (12.8)	0.495
Male Sex N (%)	42 (60.9)	41 (59.4)	1
Lines Mean (SD)	2.3 (0.9)	2.3 (0.9)	0.84
Time From Infusion Mean (SD)	821.7 (480.1)	820.7 (493.7)	0.99
Pre-treatment WBC	5.1(3.4)	5.9 (2.6)	0.126
Pre-treatment ANC	3.4 (2.9)	4.1 (2.4)	0.138
Pre-treatment ALC	0.7 (0.4)	0.9 (0.6)	0.018*
Pre-treatment Hg	10.2 (1.6)	10.7 (1.7)	0.07
Pre-treatment Plt	222.5 (86.9)	190.6 (80.9)	0.03*

Table S1: Baseline characteristics and matched variables between autologous hematopoietic cell transplantation (HCT) and chimeric antigen receptor T-cell (CAR)-treated patients. This table summarizes the variables used for propensity score matching (age, sex, systemic therapy lines, time from infusion) and pre-infusion hematologic parameters. All patients had large B-cell lymphoma (LBCL) and no history of relapse prior to matching. P-values were calculated using unpaired two-tailed t-tests or chi-square tests, as appropriate.

CCT Type	Matched	Cause of Death	Post-Infusion Day of Death
CAR	Yes	Bacteremia (pseudomonas)	1363
CAR	Yes	Pneumonia (PJP)	137
CAR	Yes	COVID Pneumonia	1205
CAR	Yes	COVID Pneumonia	705
CAR	Yes	COVID Pneumonia	839
CAR	Yes	Pneumonia (unknown)	32
CAR	Yes	EBV causing HLH	62
CAR	Yes	Myelodysplastic Syndrome	426
CAR	No	Mesothelioma	1330
CAR	NA	Fungemia (candida)	43
CAR	NA	Bacteremia (e coli)	215
CAR	NA	COVID Pneumonia	423
CAR	NA	Bacteremia (klebsiella)	21
HCT	Yes	Squamous Cell Carcinoma	946
HCT	No	Endometrial Cancer	1082

Table S2: Causes of non-relapse mortality (NRM) among patients treated with HCT or CAR therapy. Infection was the most frequent cause of NRM among CAR-treated patients. Day of death is measured from the time of infusion. Matched status indicates inclusion in the propensity-matched cohort.

Category	HCT	CAR	p
n	29	17	
Primary_Malignancy (%)			0.018
LBCL	16 (55.2)	16 (94.1)	
MCL	6 (20.7)	1 (5.9)	
TCL	7 (24.1)	0 (0.0)	
Age (median [IQR])	62.00 [57.00, 66.00]	64.00 [54.00, 70.00]	0.673
Sex = M (%)	22 (75.9)	9 (52.9)	0.202
Systemic lines (median [IQR])	3.00 [2.00, 3.00]	4.00 [3.00, 5.00]	0.002
IPSSR (median [IQR])	6.50 [4.50, 8.25]	5.50 [3.00, 7.00]	0.187
Complex Karyotype = Yes (%)	15 (55.6)	5 (33.3)	0.289
Minus 7 = Yes (%)	16 (59.3)	8 (53.3)	0.963
Minus 5 = Yes (%)	15 (55.6)	5 (33.3)	0.289

Table S3: Clinical and molecular characteristics of treatment-related myeloid neoplasms (tMN) following autologous hematopoietic cell transplantation (HCT) or chimeric antigen receptor T-cell (CAR) therapy. This table compares key features of tMN cases between the HCT and CAR cohorts, including karyotype abnormalities, Revised International Prognostic Scoring System (IPSS-R) classification, and disease subtype (myelodysplastic syndrome [MDS] vs acute myeloid leukemia [AML]). P-values were calculated using Fisher's exact test or chi-square test, as appropriate.

Gene Name	Exon Size	Exon Coverage	Percent Coverage
SF3B1	6025	6025	100
U2AF1	2637	2637	100
MYD88	4681	4681	100
TET2	36027	36027	100
DNMT3A	12447	12447	100
STAT3	11246	11246	100
TP53	8689	8611	99.10
ASXL1	10430	8122	77.87
CBL	2702	2036	75.35
SRSF2	4056	2455	60.53
IDH2	4534	1579	34.83
PPM1D	3467	1054	30.40
GNB1	2304	424	18.40
GNAS	21650	3844	17.76
JAK2	9674	1638	16.93
CHEK2	21869	2532	11.58
IDH1	4574	328	7.17

Table S4: Genes included in the clonal hematopoiesis (CH) capture-based sequencing panel and corresponding coverage metrics. The table lists targeted CH-associated genes used for variant detection, along with exon size, total exon coverage, and the percent of the coding region covered. Coverage was computed across the panel's targeted capture space and used to evaluate variant detection sensitivity across included loci.

Pre-Infusion CH	No CH	Has CH	p
n	50	52	
Age (median [IQR])	59.00 [48.00, 68.00]	67.00 [59.75, 72.00]	0.004
Sex = Male (%)	26 (53.1)	31 (59.6)	0.643
Prior Lines (median [IQR])	3.00 [2.00, 3.00]	3.00 [2.00, 3.00]	0.31
CAR Heme Tox = Low (%)	28 (57.1)	23 (44.2)	0.272
PreLD WBC (median [IQR])	5.20 [3.70, 6.70]	5.10 [3.95, 6.60]	0.777
PreLD ANC (median [IQR])	3.14 [2.12, 4.87]	3.50 [2.02, 4.88]	0.894
PreLD ALC (median [IQR])	0.68 [0.48, 0.98]	0.65 [0.46, 1.00]	0.866
PreLD HG (median [IQR])	10.50 [9.00, 12.00]	10.10 [8.60, 11.03]	0.141
PreLD PLT (median [IQR])	163.00 [115.00, 199.00]	168.00 [122.00, 199.50]	0.793

Table S5: Clinical characteristics of patients with and without detectable clonal hematopoiesis (CH) prior to CAR T-cell infusion. Patients were stratified by the presence or absence of pre-infusion CH mutations. Baseline variables including age, blood counts, and prior therapy were compared using appropriate statistical tests. P-values indicate group differences.

Paper ID	Clone ID	Percent Myeloid	Mutations Present
Patient_25	Clone 1	69.3	TP53_F270S
Patient_25	Clone 2	94.5	TP53_F270S
Patient_25	Clone 3	99.7	TP53_F270S;TP53_del
Patient_25	Clone 4	99.9	TP53_F270S;TP53_del;EZH2_E249K
Patient_102	Clone 5	24.5	DNMT3A_L547H
Patient_102	Clone 6	46.3	TET2_H1676fs
Patient_102	Clone 7	91.4	PPM1D_S412fs
Patient_180	Clone 8	45.9	DNMT3A_splicing
Patient_180	Clone 9	95.6	DNMT3A_F752del; ATM_G2020V
Patient_180	Clone 10	99.3	BCOR_V896fs
Patient_197	Clone 11	97.7	TP53_Y205*; TP53_R282W
Patient_235	Clone 12	93.5	DNMT3A_splicing
Patient_238	Clone 13	5.5	DNMT3A_R635W
Patient_238	Clone 14	21.2	DNMT3A_R882H;PPM1D_R551Nfs
Patient_238	Clone 15	30.8	DNMT3A_R882H
Patient_238	Clone 16	56.4	DNMT3A_R882H;PPM1D_E540Dfs
Patient_286	Clone 17	94.4	DNMT3A_R729W
Patient_316	Clone 18	91.9	DNMT3A_E733*
Patient_316	Clone 19	95.5	DNMT3A_T862I; TP53_splicing
Patient_316	Clone 20	95.6	DNMT3A_T862I
Patient_321	Clone 21	46.8	DNMT3A_L798P
Patient_321	Clone 22	58.1	TP53_G266V
Patient_356	Clone 23	4.2	DNMT3A_M801V
Patient_356	Clone 24	89	TET2_W1003*
Patient_356	Clone 25	90.1	PPM1D_Q524*
Patient_356	Clone 26	97.7	PPM1D_L450*
Patient_356	Clone 27	97.9	PPM1D_S570*
Patient_380	Clone 28	92	EZH2_Y741Lfs*22
Patient_380	Clone 29	98	DNMT3A_C497R

Table S6: Cell-type distribution of individual CH clones identified in post-CAR bone marrow using single-cell DNA sequencing. Each clone is annotated with its corresponding mutation profile and the fraction of total cells assigned to myeloid lineages. These data reflect lineage bias and differentiation potential of clonal hematopoiesis after CAR therapy.

Sample	Mutation 1	Mutation 2	Mutation 3
E4F4	TP53	TP53 LOH	EZH2
A3B3	TP53	TP53	
D1C1	DNMT3A	TP53	
A1B1	DNMT3A	ATM	
E1F1	DNMT3A	PPM1D	
E1F1	DNMT3A	PPM1D	

Table S7: Hierarchical structure of clonal hematopoiesis mutations in six clones harboring multiple pathogenic variants. Two patients exhibited biallelic loss of *TP53*, which was associated with development of aggressive therapy-related myeloid neoplasms (tMN). In four additional patients, a canonical DNA damage response (DDR) gene mutation emerged following an age-related CH mutation (*e.g.*, *DNMT3A* or *TET2*), consistent with chemotherapy-induced clonal evolution from a pre-existing CH clone. These patterns suggest cooperative oncogenic potential and selective advantage conferred by dual mutational events.

Part IV: Supplementary References

1. Hamilton MP, Craig E, Gentille Sanchez C, et al. CAR19 monitoring by peripheral blood immunophenotyping reveals histology-specific expansion and toxicity. Blood Advances 2024. DOI: 10.1182/bloodadvances.2024012637.

2. Ho D, Imai K, King G, Stuart EA. MatchIt: Nonparametric Preprocessing for Parametric Causal Inference. Journal of Statistical Software 2011;42(8):1 - 28. DOI: 10.18637/jss.v042.i08.

3. Teh BW, Mikulska M, Averbuch D, et al. Consensus position statement on advancing the standardised reporting of infection events in immunocompromised patients. Lancet Infect Dis 2024;24(1):e59-e68. (In eng). DOI: 10.1016/s1473-3099(23)00377-8.

4. Arber DA, Orazi A, Hasserjian RP, et al. International Consensus Classification of Myeloid Neoplasms and Acute Leukemias: integrating morphologic, clinical, and genomic data. Blood 2022;140(11):1200-1228. DOI: 10.1182/blood.2022015850.

5. Khoury JD, Solary E, Abla O, et al. The 5th edition of the World Health Organization Classification of Haematolymphoid Tumours: Myeloid and Histiocytic/Dendritic Neoplasms. Leukemia : official journal of the Leukemia Society of America, Leukemia Research Fund, UK 2022;36(7):1703-1719. DOI: 10.1038/s41375-022-01613-1.

6. Hamilton MP, Sugio T, Noordenbos T, et al. Risk of Second Tumors and T-Cell Lymphoma after CAR T-Cell Therapy. The New England journal of medicine 2024;390(22):2047-2060. DOI: 10.1056/NEJMoa2401361.

7. Good Z, Spiegel JY, Sahaf B, et al. Post-infusion CAR TReg cells identify patients resistant to CD19-CAR therapy. Nature medicine 2022;28(9):1860-1871. DOI: 10.1038/s41591-022-01960-7.

8. Spiegel JY, Patel S, Muffly L, et al. CAR T cells with dual targeting of CD19 and CD22 in adult patients with recurrent or refractory B cell malignancies: a phase 1 trial. Nature medicine 2021. DOI: 10.1038/s41591-021-01436-0.

9. Borcherding N, Bormann NL, Kraus G. scRepertoire: An R-based toolkit for single-cell immune receptor analysis. F1000Res 2020;9:47. DOI: 10.12688/f1000research.22139.2.

10. Phipson B, Sim CB, Porrello ER, Hewitt AW, Powell J, Oshlack A. propeller: testing for differences in cell type proportions in single cell data. Bioinformatics 2022;38(20):4720-4726. DOI: 10.1093/bioinformatics/btac582.

11. Subramanian A, Tamayo P, Mootha VK, et al. Gene set enrichment analysis: a knowledge-based approach for interpreting genome-wide expression profiles. Proceedings of the National Academy of Sciences of the United States of America 2005;102(43):15545-50. DOI: 10.1073/pnas.0506580102.

12. Greenberg PL, Tuechler H, Schanz J, et al. Revised International Prognostic Scoring System for Myelodysplastic Syndromes. Blood 2012;120(12):2454-2465. DOI: 10.1182/blood-2012-03-420489.

13. Nguyen-Khac F, Bidet A, Daudignon A, et al. The complex karyotype in hematological malignancies: a comprehensive overview by the Francophone Group of Hematological Cytogenetics (GFCH). Leukemia : official journal of the Leukemia Society of America, Leukemia Research Fund, UK 2022;36(6):1451-1466. DOI: 10.1038/s41375-022-01561-w.

14. Alig SK, Shahrokh Esfahani M, Garofalo A, et al. Distinct Hodgkin lymphoma subtypes defined by noninvasive genomic profiling. Nature 2024;625(7996):778-787. DOI: 10.1038/s41586-023-06903-x.

15. Sworder BJ, Kurtz DM, Alig SK, et al. Determinants of resistance to engineered T cell therapies targeting CD19 in large B cell lymphomas. Cancer cell 2022. DOI: 10.1016/j.ccell.2022.12.005.

16. Newman AM, Lovejoy AF, Klass DM, et al. Integrated digital error suppression for improved detection of circulating tumor DNA. Nature biotechnology 2016;34(5):547-555. DOI: 10.1038/nbt.3520.

17. Miles LA, Bowman RL, Merlinsky TR, et al. Single-cell mutation analysis of clonal evolution in myeloid malignancies. Nature 2020;587(7834):477-482. (In eng). DOI: 10.1038/s41586-020-2864-x.

18. Sollier E, Kuipers J, Takahashi K, Beerenwinkel N, Jahn K. COMPASS: joint copy number and mutation phylogeny reconstruction from amplicon single-cell sequencing data. Nature communications 2023;14(1):4921. DOI: 10.1038/s41467-023-40378-8.